Journal of Medicinal Chemistry

Article

pubs.acs.org/jmc

Methyl-Thiazoles: A Novel Mode of Inhibition with the Potential to Develop Novel Inhibitors Targeting InhA in *Mycobacterium tuberculosis*

Pravin S. Shirude,*[,†] Prashanti Madhavapeddi,[‡] Maruti Naik,[†] Kannan Murugan,[†] Vikas Shinde,[†] Radha Nandishaiah,[‡] Jyothi Bhat,[‡] Anupriya Kumar,[†] Shahul Hameed,[†] Geoffrey Holdgate,[#] Gareth Davies,[#] Helen McMiken,[#] Naina Hegde,[‡] Anisha Ambady,[‡] Janani Venkatraman,[‡] Manoranjan Panda,[†] Balachandra Bandodkar,[†] Vasan K. Sambandamurthy,[‡] and Jon A. Read*[,#]

[†]Department of Medicinal Chemistry, [‡]Department of Biosciences, AstraZeneca India Pvt. Ltd., Bellary Road, Hebbal, Bangalore-560024, India

[#]Discovery Sciences, AstraZeneca, Alderley Park, Macclesfield SK10 4TG, U.K.

Supporting Information

ABSTRACT: InhA is a well validated *Mycobacterium tuberculosis* (Mtb) target as evidenced by the clinical success of isoniazid. Translating enzyme inhibition to bacterial cidality by targeting the fatty acid substrate site of InhA remains a daunting challenge. The recent disclosure of a methyl-thiazole series demonstrates that bacterial cidality can be achieved with potent enzyme inhibition and appropriate physicochemical properties. In this study, we report the molecular mode of action of a lead methyl-thiazole, along with analogues with improved CYP inhibition profile. We have identified a novel mechanism of InhA inhibition characterized by a hitherto unreported "Y158-out" inhibitor-bound conformation of the protein that accommodates a neutrally charged "warhead". An additional novel hydrophilic interaction with protein residue M98 allows the incorporation of favorable physicochemical properties for cellular activity. Notably, the methyl-thiazole prefers the NADH-bound form of the enzyme with a K_d of ~13.7 nM, as against the NAD^+-bound form of the enzyme.

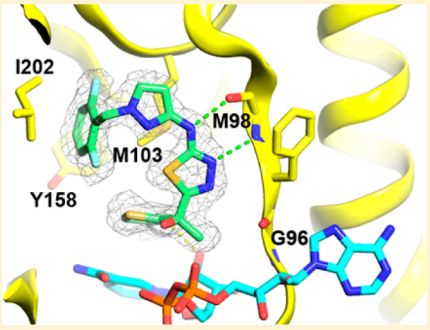

INTRODUCTION

Tuberculosis (TB) continues to be a major global cause of morbidity and mortality due to the infectious pathogen *Mycobacterium tuberculosis* (Mtb). The emergence of Mtb strains resistant to first line and second line TB drugs adds to the challenge in global efforts to control this infection.[1] The bacterial fatty acid biosynthesis pathway represents a validated and yet relatively unexploited target for drug discovery.[2] Fatty acids are essential for bacterial growth, however, they cannot be scavenged from the host and must be synthesized de novo.[3,4] In Mtb, Enoyl-acyl carrier protein reductase (ACPER), known as InhA, is encoded by the *inhA* gene as an essential NADH dependent enzyme in the mycolic acid biosynthetic pathway.[4,5] Mycolic acids are linked to the cell wall and form a waxy protective coating around the bacterial cell, which serves as a permeability barrier. The bacterial fatty acid biosynthetic pathway (FAS-II) is fundamentally distinct from the multi-enzyme FAS-I complex found in mammals. This combination results in a molecular target which is both essential in Mtb as well as sufficiently different from human enzymes to be an attractive target for small molecule drug discovery.

InhA is a clinically validated target based on the success of isoniazid (INH) in treating TB patients.[5−7] INH is a pro-drug and is activated by KatG, a catalase−peroxidase enzyme. This enzyme oxidizes INH to an acyl radical which then forms a covalent adduct (INH-NAD) with nicotinamide adenine dinucleotide (NAD).[6] The active drug is the INH-NAD covalent adduct (**1**) and one of the resistance mechanisms to INH is via a specific mutation in the KatG gene.[6] A number of additional drugs such as ethionamide and propionamide also target InhA via an adduct with cofactors.[8] Additionally, the existence of Mtb clinical isolates that harbor mutations in the *inhA* structural gene or *inhA* promoter region that confer resistance to INH have been reported. These observations imply that identifying direct inhibitors of InhA would have tremendous clinical value in combating TB, not least due to the likelihood of being devoid of cross-resistance with current therapies that target InhA via a pro-drug mechanism.[7]

Multiple molecular modes of action have been attempted to target InhA. The early success of INH in inhibiting InhA relied on targeting the NAD adduct formation which competes kinetically with the cofactor NADH. A similar mode of action has been attempted with boronate NAD adducts with limited success.[9] Mimicking the molecular mode of action of INH could be achieved either using a new pro-drug or by discovering

Received: June 26, 2013

   dx.doi.org/10.1021/jm4012033 | *J. Med. Chem.* XXXX, XXX, XXX−XXX

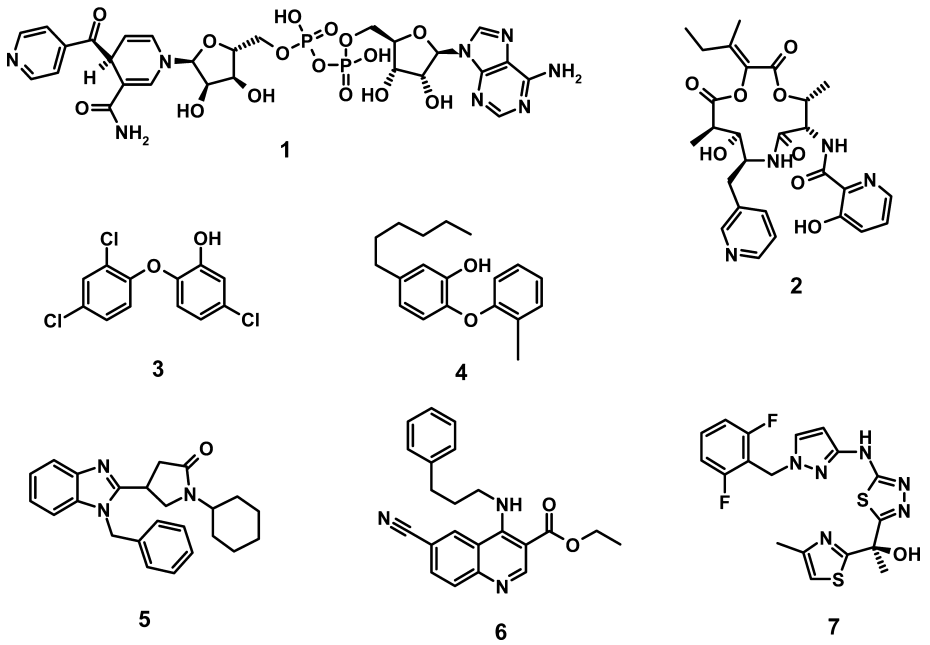

Figure 1. Chemical structures of key InhA inhibitors. **1**, isoniazid-NAD adduct (INH-NAD); **2**, pyridomycin; **3**, triclosan; **4**, PT70; **5**, benzimidazolo-pyrrolidinone; **6**, aminoquinolines; **7**, methyl thiazole.

a small molecule which would mimic **1**. The latter option poses significant issues such as the molecular weight of **1**, which is in excess of 800 Da. If analogues targeting this pathway required a similar molecular weight, this would likely limit opportunities for oral absorption.[10] The natural product **2** (pyridomycin), is reported to kill Mtb by targeting InhA.[11] Compound **2** does not show reduced activity in cell lines which are resistant to INH via mutation in KatG. Interestingly, it has been established that **2** competes with cofactor.[11] Although the complex structure of **2** with InhA has not yet been published, this result implies that **2** may act by binding in the same binding site as cofactor and **1**.

Alternative approaches for direct inhibition of InhA include allosteric modulators of InhA binding outside the active site or inhibitors that bind within the substrate binding site, thereby competing for substrate or product. To date, no allosteric inhibitors of InhA have been reported. Substrate competitive compounds, however, such as **3** (triclosan), have been known for some time. Compound **3**, a highly effective broad-spectrum antibacterial agent, targets FabI, the nonmycobacterial equivalent of InhA.[2] **3** binds directly to the NAD^+ binary complex of the enzyme and therefore does not require KatG activation for antibacterial activity.[12,13] **3** is a submicromolar (0.2 μM) inhibitor of InhA with very weak antimycobacterial activity (minimal inhibitory concentration (MIC) of 64 μM). The discovery of highly ligand efficient analogues of **3** such as **4** (PT70)[14] strengthens this approach to target InhA. However, translating enzyme inhibition to bacterial cidality while retaining the physicochemical properties required for achieving optimal bioavailability remains a significant challenge. Our efforts within AstraZeneca have led to the identification of a number of different scaffolds in this pathway including **5** (benzimidazolo-pyrrolidinone) and **6** (aminoquinolines), which lack Mtb MIC despite good enzyme inhibition (Figure 1 and Table 1). This led us to conclude that there is disconnect between enzyme inhibition and cellular potency.

Most recently in 2011, the publication of the methyl thiazole series by GlaxoSmithKline has shown that mycobacterial cellular potency (MIC) can be achieved with potent enzyme inhibition (IC_{50}). The methyl thiazole scaffold (**7**) (Figure 1) has been reported[15,16] as a direct InhA inhibitor where potent enzyme inhibition (InhA IC_{50} = 0.003 μM) translates into cellular potency (Mtb MIC = 0.19 μM) (Table 1). We have elucidated the molecular mode of action of this series and the properties that drive cellular potency. In addition, we report new analogues of the methyl thiazole series which act through a similar mode of inhibition to the reported methyl thiazoles while showing improved cytochrome P450 (CYP) inhibition and safety profile.

Table 1. IC_{50} and MIC of Key InhA Inhibitors[a]

	1	2	3	4	5	6	7
K_i (nM)	0.75	NA	NA	NA	NA	NA	NA
InhA IC_{50} (μM)	NA	6	0.2	0.022	1	0.02	0.003
MIC (μM)	0.05[b]	0.57	64	NA	>64	>64	0.19

[a]For compounds **1**–**4**: values are from literature. NA: not available. [b]MIC for INH.

RESULTS AND DISCUSSION

To understand the molecular mode of action of **7**, we profiled this compound with various techniques. These included biophysical characterization to determine the form of InhA to which the compound bound and the crystal structure determination of InhA in complex with **7** to gain a more detailed insight into the mode of action. Finally, selection mutagenesis was employed to confirm that InhA is indeed the target of these compounds. The binding affinity of **7** to InhA was shown to be dependent upon the presence of the added cofactor and its oxidation state (Figure 2, Table 2). Using isothermal titration calorimetry (ITC) and thermal melting, no binding was detected to apo InhA by **7** under the conditions used, while **7** showed weak binding to the NAD^+-bound form (9.3 μM) and tight binding to the NADH-bound form (13.7 nM). The ITC data was used primarily to determine K_d and

dx.doi.org/10.1021/jm4012033 | J. Med. Chem. XXXX, XXX, XXX–XXX

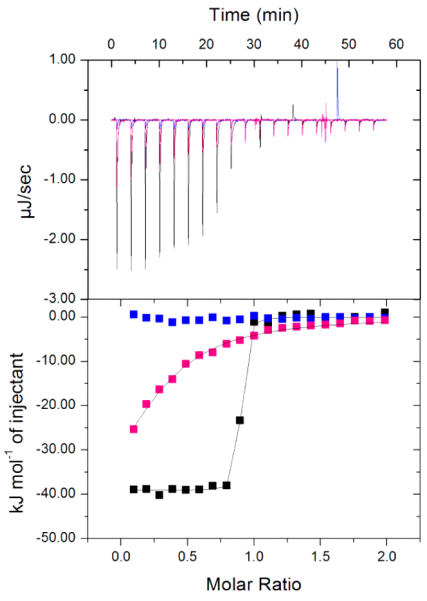

Figure 2. Isothermal titration calorimetry (ITC) data for **7** binding to InhA. Titrations of **7** with apo InhA (blue) and with NADH-bound (black) and NAD^+-bound (red) are shown.

determine the preference of the compound for E:NAD^+, E.NADH, or apo InhA. There may be multiple other reasons for the change in enthalpy/entropy such as changes in protein dynamics, changes in contribution of water molecules, entropy/enthalpy compensation, entropy/enthalpy transduction, and differential conformational changes. We have not tried to interpret these values in this context.

The binding affinity of **7** to the NADH-bound form of the enzyme, determined from surface plasmon resonance (SPR) studies is 11.5 nM (Supporting Information), agreed well with that from ITC (13.7 nM). In addition, binding affinities for NAD^+ and NADH to InhA were determined by SPR under the same conditions as described for **7**, with K_d values being 434 μM (95% confidence intervals 263−606 μM) and 5.6 μM (95% confidence intervals 5.3−5.8 μM), respectively. The binding affinity for NADH was also measured by ITC, with good agreement to the SPR derived value, with $K_d = (2.4 \pm 0.3)$ μM. Compound binding to the NADH form fits to a "one binding site per monomer" model in both ITC and SPR. It is difficult to know whether the protein is a monomer or tetramer from ITC and SPR experiments. However, the results are consistent between the two techniques. Further, the mode of inhibition was investigated using binding studies of **7** in thermal melting experiments utilizing the differential scanning fluorimetry.[17] The data shows a modest increase in thermal stability of InhA as observed on addition of either the oxidized (NAD^+) or reduced (NADH) cofactor. Titration of **7** with apo enzyme or the E.NAD^+ complex (enzyme−NAD^+ complex) resulted in no significant increase in melting temperature. However, a dramatic increase in the melting temperature of InhA is observed on the titration of **7** to the E.NADH complex (Table 2, Supporting Information Figure S1).

The ITC binding studies suggest that **7** follows uncompetitive kinetics with respect to both oxidized and reduced cofactor. Binding therefore occurs only after the cofactor has bound to the free enzyme under the assay conditions. Compound **7** binds with an approximately 1000-fold higher affinity to the E.NADH complex. The stoichiometry measured for **7** binding to the E.NADH complex was 0.86 ± 0.002. Binding of **7** can therefore be described by Scheme 1 below,

Scheme 1. Proposed Mode of Inhibition for Compound 7

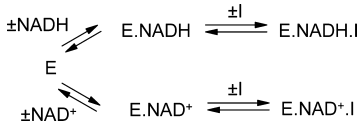

wherein the higher affinity binding to the E.NADH compared to the E.NAD^+ form suggests a mode of inhibition that may be different to the stacking interactions typical of **3** and **4** with E.NAD^+. Previous kinetic studies have revealed that substrate binds in random order,[18] suggesting that **7** could inhibit InhA by binding to E.NADH to form a ternary complex or by binding to E.NADH.S (where S refers to long chain trans 2-enoyl-acyl carrier protein (ACP) substrates) to form a quaternary complex, however, as there was no substrate present in the ITC experimental setup, we cannot distinguish between these two modes of inhibition from the ITC data alone.

These data suggest that of the two binary complex options, **7** binds to the binary E.NADH form to make a ternary complex. The thermal melting data are consistent with this hypothesis. Interestingly, estimates of intracellular concentrations of NADH and NAD^+ levels in *Mycobacteria* are similar and well above K_m for each cofactor species.[19] As K_m (NADH) is approximately 100-fold tighter than K_m (NAD^+), it could be hypothesized that binding to E.NADH would be an efficient way to inhibit a binary complex form of InhA as the vast majority of the enzyme would be in this form, assuming the estimates of intracellular cofactor concentrations are valid and that other effects such as local concentrations, are not evident. The crystal structure of InhA in complex with **7** is shown in Figure 3. Consistent with the biophysical measurements, **7** binds to the E.NAD complex and occupies the substrate

Table 2. Biophysical Measurements of 7[a]

	ITC				SPR	thermal melting			
InhA form	K_d (nM)	ΔG (kJ/mol)	ΔH (kJ/mol)	$-T\Delta S$ (kJ/mol)	K_d (nM)	T_m (°C)	T_m (°C) (apoenzyme)	ΔTm (°C)	ΔTm (°C) (cofactor bound form)
Apo	NB	n/a	n/a	n/a	NA	54.2 ± 0.22	n/a		
NAD^+	9300 ± 1100	−28.7 ± 0.3	−58.2 ± 7.1	−29.5 ± 7.1	NA	55.2 ± 0.29	+1.0	55.0 ± 0.003 (at 50 μM of **7**)	−0.2
NADH	13.7 ± 3.8	−44.9 ± 0.7	−39.3 ± 0.2	5.4 ± 0.7	11.5 ± 2.8	56.5 ± 0.11	+2.3	69.3 ± 0.20(at 50 μM of **7**)	+12.8

[a]NB: no binding. n/a: not applicable. NA: not available.

dx.doi.org/10.1021/jm4012033 | J. Med. Chem. XXXX, XXX, XXX−XXX

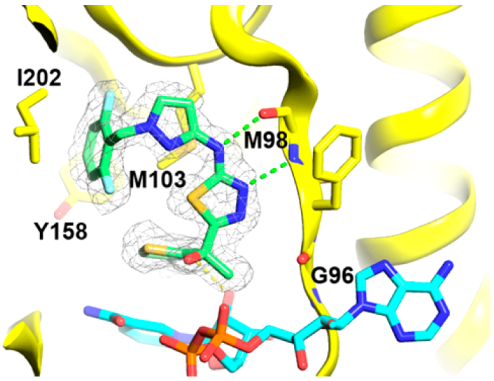

Figure 3. X-ray crystal structure (PDB ID 4bpq) of **7** bound to InhA of Mtb. Carbon atoms for **7** are shown in green. The protein backbone cartoon is represented in yellow. Selected atoms for the InhA side chains including the catalytic residue Y158 and M98 are shown as sticks. NADH is shown as sticks colored with cyan carbon atoms. Refined ($2f_o f_c$) electron density contoured at 1.0σ for **7** is represented as wire mesh. Some atoms of the active site covering loop have been removed for clarity.

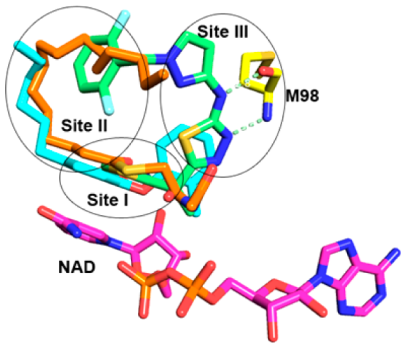

Figure 4. Substrate site binding regions of InhA. Protein complexes of **7** (PDB ID 4bpq), **4** (PDB ID 2x23),[20] and C16 fatty acyl substrate (PDB ID 1bvr)[21] are overlaid. The figure highlights three regions within the substrate binding site: site I, the catalytic site; site II, the hydrophobic pocket; site III, also termed the size-limited region.[14] Proteins atoms have been removed for clarity, except for M98 from the InhA–NADH–**7** complex which is drawn with carbon atoms in yellow. **7** is shown as sticks with green carbon atoms, **4** is shown with cyan carbon atoms, and C16 fatty acyl substrate is shown with orange carbon atoms. NAD is shown as sticks with pink carbon atoms. Both the phenolic ring of **4** and the methyl thiazole ring of **7** occupy a similar positioning, allowing π-stacking with the nicotinamide ring of the cofactor NAD.

binding site. The methyl-thiazole group engages with the nicotinamide and ribose groups of the NAD cofactor, and this interaction can be seen more clearly in Figure 5d. These specific interactions with the cofactor are in common with known substrate competitive InhA inhibitors. The site defined by ligand groups interacting with the nicotinamide ring and ribose hydroxyl in substrate competitive inhibitor complexes will be termed "site I" subsequently in this article. The thiazole ring "N" acts as a hydrogen bond acceptor to the hydroxyl group of the ribose of the cofactor NADH. The thiazole ring itself π-stacks with the nicotinamide ring of NADH. Uniquely among known InhA substrate competitive inhibitors, the methyl group of the methyl thiazole forces Y158 to maintain a "flipped out" conformation by preventing the residue from adopting an active "flipped in" conformation as seen in all previously reported substrate competitive InhA inhibitors. The geometry of the tetrahedral carbon adjacent to the thiazole ring allows the remainder of the molecule to curl away from a path approximately parallel with NADH and avoid steric clashes with the protein, namely the main chain of G96.

A unique H-bond donor–acceptor pair is formed between a thiadiazole ring nitrogen and the amine "NH" between the thiadiazole and pyrazole rings with the M98 backbone amide "NH" and carbonyl "O", respectively. This interaction is also previously unreported in crystal structures of InhA with inhibitors. The orientation of this donor–acceptor hydrogen bond pairing provides an excellent vector for the introduction of a linking pyrazole which allows the difluoro-phenyl ring to access a hydrophobic pocket. The hydrophobic pocket accommodates the alkyl chain of the InhA substrate during the InhA catalytic cycle (Figure 4). The thiadiazole, pyrazole, and phenyl rings of **7** wrap around the side chain of M103. Finally, the active site loop of InhA (residues 198–206), a helix which may be disordered or ordered in crystal structures of InhA dependent on interactions with ligand, makes nonpolar contacts between M199 and the methyl-thiazole sulfur, I202 and the phenyl ring. The loop is fully ordered in subunits A–D, and density is weaker in subunits E and F. The crystal structure of the complex between InhA and **7** correlates well with biophysical analysis. The structure is consistent with the compound binding to a binary complex of InhA. At 2.0 Å, the resolution is not sufficient to determine whether the cofactor is present in a reduced or oxidized state. From this point onward, NAD will be used to denote cofactor when either the actual redox state is not confirmed or the statement refers equally to NAD^+ or NADH. However, the crystals were soaked in reduced NADH cofactor concomitant with the introduction of **7**. As it had previously been shown that cofactor can be soaked out of and into this crystal form (unpublished results), it can be assumed that the cofactor in this crystal is in the reduced (NADH) form.

The InhA substrate binding site can be divided into three key regions that substrate-competitive inhibitors occupy and which are highlighted in Figure 4. In **3**[23] and **4**,[20] site I contains phenolic oxygen which is often linked to a ring system which stacks with the nicotinamide group. In other ligands, such as the pyrrolidine carboxamides,[22] the ring at site I is not aromatic and the oxygen engaging with the ribose at site I need not be directly attached to a ring as demonstrated by the piperazine-indole-formamide compound GENZ10850 (PDB ID 1p44)[13] or the natural fatty acid substrate. Prior to the identification of **7**, all substrate-competitive inhibitors with known binding mode possessed an oxygen atom that interacts with the ribose ring and the hydroxyl of Y158. This interaction with Y158 will be discussed further below. Site II is a hydrophobic pocket that accommodates the long alkyl chains of the substrate.[21] The pocket is flexible due to significant movements in the side chains of a few key residues such as Y158 and F149 and large movements in the substrate-binding loop (amino acids 196–208). Flexibility within the hydrophobic pocket is exploited in InhA substrate-competitive inhibitors. Notably **3**, a moderately potent inhibitor of InhA, does not exploit this pocket.[23] While extending into the hydrophobic pocket provides benefit by increasing potency, it also has the effect of significantly increasing lipophilicity. A third and relatively unexplored region, site III is located to the top right of Figure 4. This region presents the opportunity for hydrophilic interactions with M98 as well as the placement of hydrophilic groups (in this case a hydroxyl group) adjacent to the phosphate groups of

dx.doi.org/10.1021/jm4012033 | J. Med. Chem. XXXX, XXX, XXX–XXX

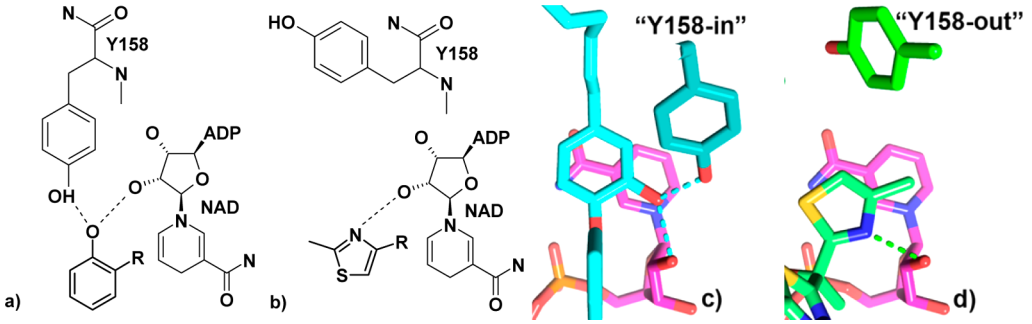

Figure 5. InhA catalytic site I interactions: (a,b) diagrammatic representation of chemical structures and (c,d) stick representations of X-ray crystal structures representing two classes of catalytic site interactions. Substrate competitive inhibitors have been categorized into two types by their interactions at site I according to the conformation of tyrosine residue 158; "Y158-in" (a,c) as demonstrated by **4**[20] and a previously unreported "Y158-out" conformation (b,d) as demonstrated by the complex of **7** with InhA.

Table 3. Methyl-thiazoles Are Potent Inhibitors of InhA and Inhibit the Growth of Replicating Mtb in Broth

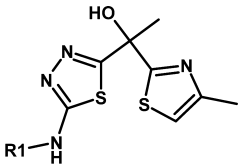

No	R1	InhA IC_{50} (μM)	Mtb MIC (μM)	No	R1	InhA IC_{50} (μM)	Mtb MIC (μM)
8	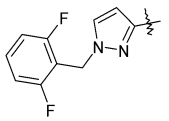	0.004	0.5	**13**	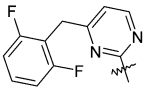	<0.002	12.5
9	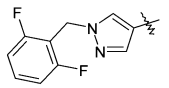	0.234	7.5	**14**	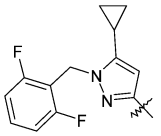	0.97	>12.5
10	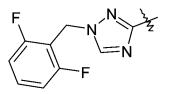	0.03	<0.391	**15**	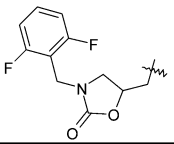	0.4	>100
11	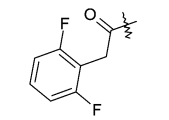	0.20	3.75	**16**	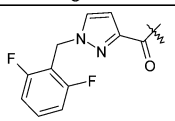	34	>100
12	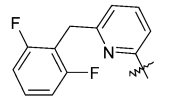	<0.002	3.13				

NAD. These unexplored features of the InhA binding pocket present a significant opportunity to modulate the physicochemical properties of InhA binding molecules.

In the "Y158-in" binding mode, the ligand has an atom which is capable of simultaneously forming a polar interaction with both a ribose hydroxyl and the Y158 phenolic hydroxyl. The "Y158-out" binding mode retains the interaction of the ligand with the ribose hydroxyl group; however, Y158 adopts an alternative $\chi 1$ torsion angle similar to the apo form of the enzyme, preventing the tyrosine phenolic oxygen from interacting with the ligand. Both Y158-in and Y158-out inhibitors often have aromatic rings which can form π-stacking interactions with the nicotinamide ring of NAD (exceptions are pyrrolidine carboxamides[22] and piperazine indole formamides[13]). In Figure 5c,d, NAD is represented with pink carbon atoms. Compound **4** is represented with cyan carbon atoms and **7** with light-green carbon atoms. Y158 carbon atoms are in blue or green.

Triclosan analogues such as **4** have been reported to bind preferentially to the NAD^+ form of InhA.[20] Compound **3** and by analogy **4**, mimics the enolate anion of the substrate[12] of ACPER and is probably present in the complex as a phenolic anion[24] (calculated $pK_a = 7.9$) at physiological pH.[14] This likely contributes to affinity by complementing the charge on the

dx.doi.org/10.1021/jm4012033 | J. Med. Chem. XXXX, XXX, XXX−XXX

oxidized NAD^+ cofactor. In addition, the phenolic oxygen allows triclosan or PT70 to make a bidentate interaction with the hydroxyl of Y158, which adopts the Y158-in conformation, and an NAD^+ ribose hydroxyl. While the charge complementarity may contribute to the potency of these compounds, it may be a factor in the poor permeability and bioavailability of such compounds.

An overlay of the complex structures of InhA with compounds **4** and **7** is shown in Figure 4. The binding mode of the methyl-thiazole at site I is novel with respect to the binding motif around the nicotinamide and adjacent ribose groups of the NAD cofactor and the interactions with Y158 of the protein and is shown more clearly in Figure 5. In the complex of **7** with InhA, there is a single hydrogen bond between the acceptor "N" on the thiazole ring and the ribose of NAD. The methyl group of **7** prevents Y158 from rotating inward, and Y158 remains in the "Y158-out" conformation as seen in the binary form of the InhA:NAD complex with **7** (Figure 5) and the apo structure of InhA[25] (PDB ID 1eny). All previously identified substrate competitive inhibitors have a binding mode similar to **3** and **4**, i.e., Y158-in.[26] In contrast to a charged Y158-in inhibitor, an inhibitor which binds to the "Y158-out" conformation of the E.NADH form of InhA could accept a hydrogen bond from the ribose hydroxyl but would be uncharged.

Keeping these interactions and considerations in mind, we designed and synthesized new analogues in order to understand structure–activity relationships (SAR), as shown in Table 3. All new analogues were racemic. Compound **8** shows similar enzyme inhibition as that of its chiral analogue **7**, however, the MIC is 2-fold weaker (0.5 μM) than **7**. In **9**, moving the "N" of the pyrazole ring as compared to **7** resulted in weaker IC_{50} and MIC. Introduction of an additional "N" in the pyrazole ring, to yield a triazole in **10**, showed much better enzyme inhibition (0.03 μM) and cellular potency (<0.39 μM). Pyrazole amines are known to inhibit CYP enzymes. We therefore decided to investigate bioisosteric replacements for the triazole ring in **10** as well as changing the pyrazole ring to the open amide in **11**. Compound **11** with the open amide is a new lead with good enzyme inhibition and cellular potency. The crystal structure of InhA in complex with **11** (Figure 6) revealed similar interactions to that of **7** (Figure 3). The methyl thiazole and thiadiazole groups form identical hydrogen bonding interactions with the ribose hydroxyl of NAD and the backbone amide of M98, respectively. The major difference in binding occurs at the difluorophenyl group. In the complex of **7** with InhA, the difluorophenyl group penetrates into the hydrophobic pocket of InhA. In the complex of **11** with InhA, the conformation of the difluorophenyl group is restricted by the amide linkage between the thiadiazole and the difluorophenyl group. This orients the difluorophenyl group toward solvent rather than toward the hydrophobic pocket. The active site loop which is ordered only in subunits A and D has minimal changes with respect to the conformation in complex with **7**. The most notable change is a rotation of the $\chi 1$ torsion angle in I202, which is required to accommodate the phenyl ring. These suboptimal interactions (i.e., loss of interaction with the hydrophobic pocket) are reflected in the weaker binding affinity of **11** for InhA vs that of compound **7**. Compounds **12** and **13** are bioisosteric replacements of the pyrazole in **8**, where the pyrazole ring is replaced with basic pyridine and pyrimidine rings, respectively. Both **12** and **13** showed good enzyme potency, however, they showed weaker cellular potency as compared to **8**. Substitution of a cyclopropyl group on the pyrazole ring in **14** resulted in poor enzyme inhibition and thus weaker cellular activity. Introduction of a methyl oxazolidinone in place of the pyrazole ring in **15** retained enzyme inhibition but lost cellular potency, possibly due to permeability or efflux issues. Compound **16**, where the pyrazole amine was replaced with a pyrazole amide, lost both enzyme and cellular potency. This may be due to the additional carbonyl group, which in combination with the pyrazole and difluorophenyl rings prevents an optimal conformation of the compound for binding to InhA.

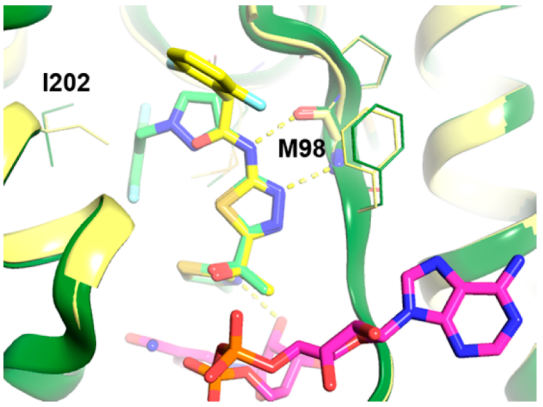

Figure 6. Overlay of X-ray crystal structures of InhA in complex with **7** (green) (PDB ID 4bpq) and **11** (yellow) (PDB ID 4bpr). Compounds **7** and **11** are shown as sticks. Protein backbone is shown as a cartoon with selected residues surrounding the substrate binding site shown as sticks. NAD is shown as sticks with magenta carbon atoms. Hydrogen bonds between the compounds and InhA and NAD are shown as yellow dotted lines.

We also profiled compounds **10** and **11** in preliminary DMPK (drug metabolism and pharmacokinetics) and safety assays and compared them with **7** (Table 4). The solubility for **10** and **11** were lower than **7**, which can be attributed to the amide group in **11**. The chiral isomers of **10** and **11** may possess better solubility as observed for **7** in comparison with its racemic analogue, **8** (data not shown). The plasma protein binding (PPB) for **10** was much better with 14% free, while **7** and **11** were similar with values between 2% and 4%. The clearance (CL) based on predicted percent liver blood flow (LBF) for **7** and **10** was in the moderate to high range for human microsomes and rat hepatocytes, respectively, however, **11** was much improved with clearance based on percent LBF of 4.5 and 7.1 for human microsomes and rat hepatocytes, respectively. The permeability measured by using a Caco-2 assay suggested that these compounds are highly permeable with no efflux. The CYP inhibition data showed significant inhibition of CYP 3A4 for **7** (1.9 μM), while **10** and **11** showed much improved profiles with CYP 3A4 inhibition 48 and >50 μM, respectively. The mammalian cytotoxicity (MMIC) against the A549 cell line was much cleaner for **10** and **11** (>100 μM), suggesting that compounds in the series are selective for bacteria and inactive on eukaryotes, while **7** showed MMIC of 78 μM. Compounds **10** and **11** were tested in 98 off-target assays were active in fewer than five targets at 30 μM (Table 4). On the basis of the observed moderate to high clearance for **10** and moderate MIC for **11**, these compounds were not tested for in vivo pharmacokinetic and efficacy study. Further medicinal chemistry efforts are required to optimize pharma-

dx.doi.org/10.1021/jm4012033 | J. Med. Chem. XXXX, XXX, XXX–XXX

Table 4. Properties of 10 and 11 in Comparison with 7

	7	10	11
InhA IC_{50} (μM)	0.003	0.03	0.2
Mtb MIC (μM)	0.195	<0.391	3.75
MMIC (μM)	78	>100	>100
aqueous solubility (μM)	208	69	26
human CL % LBF_{pred} (microsomal)	34.9	48	4.5
rat CL % LBF_{pred} (hepatocytes)	35.2	38	7.1
PPB (% free)	3.4	14.3	1.9
human Caco-2 A−B/B−A	35/21	28/27	27/17
Cyp3A4 IC_{50} (μM)	1.9	48	>50
secondary pharmacology hits[a]	ND[b]	AT, A1, and A3	A1, PDE4, 5HT2B

[a]Additional information in Supporting Information Table S1 [b]ND: not determined.

cokinetic properties and desirable cellular potency into a set of molecules to enable in vivo efficacy testing.

Having established the mechanism of inhibition using biophysical studies, we embarked on confirming the molecular target for methyl-thiazoles by generation of spontaneous resistant mutants to the parent compound. Single-step mutants arose at a frequency of 3×10^{-9} following exposure of Mtb cells to increasing concentrations of 7 (Table 5). These resistant

Table 5. MIC Values for Selected Compounds against Wild-Type and Resistant Strains of Mtb

		mutation			
compd	unit	wild-type	M103I	M103L	G96V
isoniazid	μg/mL	0.03	0.06	0.03	0.06
rifampicin	μg/mL	0.007	0.007	0.007	0.01
moxifloxacin	μg/mL	0.12	0.12	0.12	0.12
7	μM	0.39	>25	>25	>25
10	μM	1.56	>25	>25	>25

mutants displayed a greater than 64-fold increase in MIC to the parent compound in comparison to the MIC against wild-type Mtb H37Rv. There was no change in MIC to other standard drugs acting through different mechanism of action, indicating the specificity of this genetic mutation. Sequencing of the *inhA* gene from these mutants revealed a single amino acid substitution in each case resulting in three different mutations G96V, M103L or M103I (Table 5). This mutation data provides strong genetic evidence of target engagement by 7 and highlights the genetic basis for resistance. In addition to the correlation with biophysical data, the functional impact of the mutations identified by mutant selection is neatly explained by the crystal structure of 7 in complex with InhA (see Figure 3). The mutation of G96 to any other residue, including valine, would result in a clash with the linker region adjacent to the methyl-thiazole warhead. As the thiadiazole, pyrazole, and phenyl rings pack closely around M103, it is not surprising that a change of this residue to a branched leucine or isoleucine would alter the ability of the methyl-thiazole compounds to bind to InhA.

CONCLUSION

In conclusion, we report the molecular mode of action of the known Mtb InhA methyl-thiazoles. We have identified for the first time a mechanism of InhA inhibition which shows a hitherto unknown neutrally charged "warhead" being accommodated in the "Y158-out" conformation at site I of the InhA protein. Notably, these compounds show preferential binding to the NADH-bound form of the enzyme as opposed to the NAD^+ bound form of the enzyme which may well reflect the charge complementarity between the site I group and NADH (i.e., both neutral). Additionally, the current study indicates that novel hydrophilic interactions with the protein at site III lead to favorable physicochemical properties, resulting in cellular activity. On the basis of this mechanism, we have synthesized new analogues with potent enzyme inhibition, attractive cellular potency, improved CYP inhibition, and safety profile as compared to the known methyl-thiazole lead molecule, 7. Furthermore, we believe that aspects of the binding mode and molecular mode of inhibition of this series that we have reported are transferable to other series, opening up new avenues of medicinal chemistry against this important and clinically validated TB target.

EXPERIMENTAL SECTION

All anhydrous solvents, reagent grade solvents for chromatography and starting materials were purchased from either Sigma Aldrich Chemical Co. or Fisher Scientific. Water was distilled and purified through a Milli-Q water system (Millipore Corp., Bedford, MA). General methods of purification of compounds involved the use of silica cartridges purchased from Grace Purification Systems. The reactions were monitored by TLC on precoated Merck 60 F254 silica gel plates and visualized using UV light (254 nm). All compounds were analyzed for purity by HPLC and characterized by ^{1}H NMR using Bruker 300 MHz NMR and/or Bruker 400 MHz NMR spectrometers. Chemical shifts are reported in ppm (δ) relative to the residual solvent peak in the corresponding spectra; chloroform δ 7.26, methanol δ 3.31, DMSO-d_6 δ 3.33, and coupling constants (J) are reported in hertz (Hz) (where s = singlet, bs = broad singlet, d = doublet, dd = double doublet, bd = broad doublet, ddd = double doublet of doublet, t = triplet, tt = triple triplet, q = quartet, m = multiplet) and analyzed using ACD NMR data processing software. Mass spectra values are reported as m/z.

All reactions were conducted under nitrogen unless otherwise noted. Solvents were removed in vacuo on a rotary evaporator. All final compounds were purified by reverse phase HPLC or otherwise stated with >95% purity.

Abbreviations: NMP = *N*-methyl pyrrolidine, HCl = hydrochloric acid, DMF = *N*,*N*-dimethylformamide, DCM = dichloromethane, NaH = sodium hydride, ES = electrospray ionization, HRMS = high resolution mass spectrometry, RT = room temperature, RB = round-bottom; h = hour.

(1*S*)-1-(5-{ [1-(2,6-Difluorobenzyl)-1*H*-pyrazol-3-yl]amino}-1,3,4-thiadiazol-2-yl)-1-(4-methyl-1,3-thiazol-2-yl)ethanol (7). In a 100 mL single-necked RB flask was taken 1-(2,6-difluorobenzyl)-3-isocyanato-1*H*-pyrazole(200 mg, 8.50 mmol) and 2-hydroxy-2-(4-methylthiazol-2-yl)propanehydrazide (172 mg, 8.50 mmol). Ethanol (10 mL) was added to get a clear solution. The reaction mass was heated under reflux for 2 h. The desired compound was

dx.doi.org/10.1021/jm4012033 | J. Med. Chem. XXXX, XXX, XXX−XXX

confirmed by LCMS. Reaction mixture was evaporated to dryness. The residue was cooled in ice-bath and added concd sulphuric acid (5 mL) cautiously. The dark color reaction mixture was stirred at RT for 5 h. After the completion of the reaction, the reaction mass was diluted with ice water and neutralized with aqueous ammonia. The aqueous phase was extracted with ethyl acetate and washed with water and brine solution. The organic layer was separated, dried over sodium sulfate, and evaporated at high vacuum to give the crude compound which was purified by column chromatography using methanol/DCM. This compound was subjected for chiral reverse phase HPLC.

Analytical chiral conditions: CHIRALPAK-IA; dimension, 30 mm × 250 mm; 5 μ; mobile phase A, hexane; mobile phase B, 1:1 methanol:2-propanol; additive 0.1% diethylamine; flow rate 40 mL/min; temperature 40 °C; outlet pressure 100 bar; detection 280 nm; loading 100 mg/injn; concentration 50 mg/mL; diluent 4:1 methanol/THF. Optical rotation +118. ^{1}H NMR (300 MHz, DMSO-d_6) δ ppm 10.87 (br s, 1 H), 7.71 (d, J = 2.26 Hz, 1 H), 7.35−7.57 (m, 1 H), 7.29 (s, 1 H), 7.24 (d, J = 0.94 Hz, 1 H), 7.11 (t, J = 7.91 Hz, 2 H), 5.94 (d, J = 2.26 Hz, 1 H), 5.27 (s, 2 H), 2.24−2.39 (m, 3 H), 1.98 (s, 3 H), 1.04 (d, J = 6.03 Hz, 1 H). [ES + MS] m/z 436.1 (M + 1). HRMS calculated for $C_{18}H_{16}F_2N_6OS_2$, 435.0879; found, 435.0875.

1-(5-(1-(2,6-Difluorobenzyl)-1*H*-pyrazol-3-ylamino)-1,3,4-thiadiazol-2-yl)-1-(4-methylthiazol-2-yl)ethanol (8). In a 100 mL single-necked RB flask was taken 1-(2,6-difluorobenzyl)-3-isocyanato-1*H*-pyrazole (200 mg, 8.50 mmol) and 2-hydroxy-2-(4-methylthiazol-2-yl)propanehydrazide (172 mg, 8.50 mmol). Ethanol (10 mL) was added to get a clear solution. The reaction mass was heated under reflux for 2 h. The desired compound was confirmed by LCMS. Reaction mixture was evaporated to dryness. The residue was cooled in ice-bath and concd sulphuric acid (5 mL) was added cautiously. The dark color reaction mixture was stirred at RT for 5 h. After the completion of the reaction, the reaction mass was diluted with ice water and neutralized with aqueous ammonia. The aqueous phase was extracted with ethyl acetate and washed with water and brine solution. The organic layer was separated, dried over sodium sulfate, and evaporated at high vacuum to give the crude compound which was purified by column chromatography using methanol/DCM. ^{1}H NMR (300 MHz, DMSO-d_6) δ ppm 10.88 (br s, 1 H), 7.71 (d, J = 2.07 Hz, 1 H),7.36−7.55 (m, 1 H), 5.26 (s, 2 H), 7.29 (s, 1 H), 7.24 (s, 1 H), 7.11 (t, J = 7.91 Hz, 2 H), 5.93 (d, J = 2.07 Hz, 1 H), 2.30 (s, 3 H), 1.98 (s, 3 H). [ES + MS] m/z 436.1 (M + H). HRMS calculated for $C_{18}H_{16}F_2N_6OS_2$, 435.0879; found, 435.0875.

1-(5-(1-(2,6-Difluorobenzyl)-1*H*-pyrazol-4-ylamino)-1,3,4-thiadiazol-2-yl)-1-(4-methylthiazol-2-yl)ethanol (9). To a solution of 1-(2,6-difluorobenzyl)-4-isothiocyanato-1*H*-pyrazole (450 mg, 1.79 mmol) in DCM (10 mL) was added 2-hydroxy-2-(4-methylthiazol-2-yl)propanehydrazide (360 mg, 1.79 mmol) and stirred for 30 min at RT. The colorless solid was filtrated under vacuum and dried to get *N*-(1-(2,6-difluorobenzyl)-1*H*-pyrazol-4-yl)-2-(2-hydroxy-2-(4-methylthiazol-2-yl)propanoyl)hydrazinecarbothioamide (450 mg, 55.5%) as a solid. [ES + MS] m/z = 453 (M + 1). In a 10 mL of RB flask, *N*-(1-(2,6-difluorobenzyl)-1*H*-pyrazol-4-yl)-2-(2-hydroxy-2-(4-methylthiazol-2-yl)propanoyl)hydrazinecarbothioamide (200 mg, 0.44 mmol) was added followed by concd sulfuric acid (2 mL) and stirred for 30 min. The reaction mixture was neutralized carefully with aqueous ammonia solution at 0 °C. The reaction mixture was extracted with DCM, and the combined organic layer was washed with water and brine solution, dried over sodium sulfate, and concentrated under vacuum. The crude compound was purified by column chromatography to get 1-(5-(1-(2,6-difluorobenzyl)-1*H*-pyrazol-4-ylamino)-1,3,4-thiadiazol-2-yl)-1-(4-methylthiazol-2-yl)ethanol (40.0 mg, 20.83%) as a solid. ^{1}H NMR (300 MHz, DMSO-d_6) δ ppm 10.06 (s, 1H), 7.99 (s, 1H), 7.41−7.54 (m, 1H), 7.38 (s, 1H), 7.21 (d, J = 0.9 Hz, 1H), 7.15 (t, J = 8.0 Hz, 2H), 5.35 (s, 2H), 2.30 (s, 3H), 1.96 (s, 3H). [ES + MS] m/z = 435 (M + 1). HRMS calculated for $C_{18}H_{16}F_2N_6OS_2$ 435.0867; found: 435.086.

1-(5-(1-(2,6-Difluorobenzyl)-1*H*-1,2,4-triazol-3-ylamino)-1,3,4-thiadiazol-2-yl)-1-(4-methylthiazol-2-yl)ethanol (10). To a solution of 1-(2,6-difluorobenzyl)-3-isothiocyanato-1*H*-1,2,4-triazole (360 mg, 1.43 mmol) in DCM (10 mL) was added 2-hydroxy-2-(4-methylthiazol-2-yl)propanehydrazide (287 mg, 1.43 mmol) and stirred for 30 min at RT. The reaction mixture was concentrated under vacuum, and the resultant crude compound was purified by column chromatography to get *N*-(1-(2,6-difluorobenzyl)-1*H*-1,2,4-triazol-3-yl)-2-(2-hydroxy-2-(4-methylthiazol-2-yl)propanoyl) hydrazine carbothioamide (300 mg, 46.4%) as a solid. [ES + MS] m/z = 454 (M + 1). In a 25 mL of RB flask, *N*-(1-(2,6-difluorobenzyl)-1*H*-1,2,4-triazol-3-yl)-2-(2-hydroxy-2-(4-methylthiazol-2-yl)propanoyl)-hydrazinecarbothioamide (300 mg, 0.66 mmol) was added followed by concd sulfuric acid (2 mL) and stirred for 30 min. The reaction mixture was neutralized carefully with aqueous ammonia solution at 0 °C. The reaction mixture was extracted with DCM, and the combined organic layer was washed with water and brine solution, dried over sodium sulfate, and concentrated under vacuum. The crude compound was purified by column chromatography and then triturated with diethyl ether to get 1-(5-(1-(2,6-difluorobenzyl)-1*H*-1,2,4-triazol-3-ylamino)-1,3,4-thiadiazol-2-yl)-1-(4-methylthiazol-2-yl)ethanol (50.0 mg, 17.36%) as a solid. ^{1}H NMR (300 MHz, DMSO-d_6) δ ppm 11.56 (br s, 1H), 8.55 (s, 1H), 7.43−7.55 (m, 1H), 7.36 (s, 1H), 7.23 (d, J = 0.9 Hz, 1H), 7.15 (t, J = 8.0 Hz, 2H), 5.39 (s, 2H), 2.29 (s, 3H), 1.98 (s, 3H). [ES + MS] m/z = 436 (M + 1). HRMS calculated for $C_{17}H_{15}F_2N_7OS_2$, 436.082; found, 436.08.

2-(2,6-Difluorophenyl)-*N*-(5-(1-hydroxy-1-(4-methylthiazol-2-yl)ethyl)-1,3,4-thiadiazol-2-yl)acetamide(11). In a 10 mL RB flask, 2-(2,6-difluorophenyl)acetic acid (300 mg, 1.74 mmol) was heated with thionyl chloride (1.5 mL, 17.43 mmol) at 60 °C for 30 min. Then the reaction mixture was evaporated under vacuum. The resultant crude compound was dissolved in acetone (5 mL) and potassium thiocyanate (186 mg, 1.92 mmol) was added. The reaction mixture was stirred for 2 h. Then 2-hydroxy-2-(4-methylthiazol-2-yl)propanehydrazide (351 mg, 1.74 mmol) was added and stirred for another 30 min at RT. The formation of desired product was confirmed by LCMS. The reaction mixture was concentrated under vacuum to get crude 2-(2,6-difluorophenyl)-*N*-(2-(2-hydroxy-2-(4-methylthiazol-2-yl)propanoyl)hydrazinecarbonothioyl)acetamide (210 mg, 29.1%) as a gum. [ES + MS] m/z = 415 (M + 1). In a 25 mL RB flask, 2-(2,6-difluorophenyl)-*N*-(2-(2-hydroxy-2-(4-methylthiazol-2-yl)propanoyl)hydrazinecarbonothioyl)acetamide (200 mg, 0.48 mmol) was added followed by concd sulfuric acid (2 mL) and stirred for 30 min. The reaction mixture was neutralized carefully with aqueous ammonia solution at 0 °C. The reaction mixture was extracted with DCM, and the combined organic layer was washed with water and brine solution, dried over sodium sulfate, and concentrated under vacuum. The crude compound was purified by column chromatography and then triturated with diethyl ether to get 2-(2,6-difluorophenyl)-*N*-(5-(1-hydroxy-1-(4-methylthiazol-2-yl)ethyl)-1,3,4-thiadiazol-2-yl)acetamide (90 mg, 47.0%) as a solid. ^{1}H NMR (300 MHz, DMSO-d_6) δ ppm 12.91 (s, 1H), 7.50 (s, 1H), 7.35−7.47 (m, 1H), 7.23 (d, J = 0.9 Hz, 1H), 7.06−7.18 (m, 2H), 3.91 (s, 2H), 2.30 (s, 3H), 2.02 (s, 3H). [ES + MS] m/z = 397 (M + 1). HRMS calculated for $C_{16}H_{14}F_2N_4O_2S_2$, 397.0598; found, 397.0605.

1-(5-(6-(2,6-Difluorobenzyl)pyridin-2-ylamino)-1,3,4-thiadiazol-2-yl)-1-(4-methylthiazol-2-yl)ethanol (12). In a 100 mL single-necked flask equipped with an air condenser connected to nitrogen source was taken 2-(2,6-difluorobenzyl)-6-isothiocynatopyridine (200 mg, 0.763 mmol). DCM (20 mL) was added to get a clear solution. Then 2-hydroxy-2-(4-methylthiazol-2-yl)propanehydrazide (180 mg, 0.90 mmol) was added and stirred at RT for 3 h. After the completion of the reaction, the volatiles were evaporated to get the solid, which was taken in concd sulfuric acid (10 mL) and stirred at RT for 1 h. After completion of the reaction, it was neutralized with aqueous ammonia solution. The aqueous layer was extracted with ethyl acetate and washed with water and brine solution. The organic layer was separated, dried over sodium sulfate, and evaporated to get the crude compound which was purified by column chromatography using methanol/DCM to get 100 mg (27.63%) of the final compound. ^{1}H NMR (300 MHz, DMSO-d_6) δ ppm 11.50 (s, 1 H), 7.60−7.70 (m, 1 H), 7.25−7.30 (m, 1H), 7.15−7.20 (m, 2H), 6.95−7.05 (m, 2H), 6.80−6.90 (m, 2H), 4.00 (s, 2H), 2.20 (s, 3H), 1.95 (s, 3H). [ES +

dx.doi.org/10.1021/jm4012033 | J. Med. Chem. XXXX, XXX, XXX−XXX

MS] m/z = 446 (M + 1). HRMS calculated for $C_{20}H_{17}F_2N_5OS_2$, 446.0915; found, 446.09.

1-(5-(4-(2,6-Difluorobenzyl)pyrimidin-2-ylamino)-1,3,4-thiadiazol-2-yl)-1-(4-methyl thiazol-2-yl)ethanol (13). 4-(2,6-Difluorobenzyl)-2-isocyanatopyrimidine (200 mg, 0.809 mmol) was taken in a 100 mL single-necked flask equipped with an air condenser connected to nitrogen source. DCM (10 mL) was added to get a clear solution, followed by 2-hydroxy-2-(4-methylthiazol-2-yl)-propanehydrazide (162.9 mg, 0.809 mmol). The reaction mass was stirred at RT for 2 h. After completion of the reaction, the volatiles were evaporated to get the residue *N*-(4-(2,6-difluorobenzyl)-pyrimidin-2-yl)-2-(2-hydroxy-2-(4-methylthiazol-2-yl)propanoyl) hydrazine carbothioamide. The above residue (300 mg, 0.64 mmol) was taken in concd sulfuric acid (5 mL) and stirred at RT for 2 h. After the completion of the reaction, it was neutralized with aqueous ammonia and the aqueous was extracted with ethyl acetate and washed with water and brine solution. The organic layer was dried over sodium sulfate and evaporated to get the crude compound, which was purified by column chromatography using methanol/DCM as eluent to get 110 mg (30.45%) of the desired compound. ^{1}H NMR (300 MHz, DMSO-d_6) δ ppm 12.00 (s, 1H), 8.50(s, 1H), 7.30−7.45 (m, 2 H), 7.25 (s, 1 H), 7.05−7.15 (m, 2 H), 6.90−7.00 (m, 1 H), 4.10 (s, 2H), 2.30 (s, 3 H), 2.04 (s, 3 H). [ES + MS] m/z = 447 (M + 1). HRMS calculated for $C_{19}H_{16}F_2N_6OS_2$, 447.0867; found, 447.0887.

1-(5-((5-Cyclopropyl-1-(2,6-difluorobenzyl)-1*H*-pyrazol-3-yl)amino)-1,3,4-thiadiazol-2-yl)-1-(4-methylthiazol-2-yl)-ethanol (14). 5-Cyclopropyl-1-(2,6-difluorobenzyl)-3-isothiocyanato-1*H*-pyrazole (200 mg, 0.69 mmol) was taken in a 100 mL single-necked flask equipped with an air condenser connected to nitrogen source. DCM (10 mL) was added to get a clear solution followed by 2-hydroxy-2-(4-methylthiazol-2-yl)propanehydrazide (138 mg, 0.69 mmol). The reaction mass was stirred at RT for 2 h. After completion of the reaction, the volatiles were evaporated to get the residue (*N*-(5-cyclopropyl-1-(2,6-difluorobenzyl)-1*H*-pyrazol-3-yl)-2-(2-hydroxy-2-(4-methylthiazol-2-yl)propanoyl)hydrazinecarbothioamide). The above residue (300 mg, 0.61 mmol) was taken in concd sulfuric acid (5 mL) and stirred at RT for 2 h. After completion of the reaction, it was neutralized, solid obtained, filtered, washed with water, and dried. The compound was purified by column chromatography using methanol/DCM as eluent. ^{1}H NMR (300 MHz, DMSO-d_6) δ ppm 7.31−7.54 (m, 2 H), 7.24 (s, 1 H), 7.06 (t, J = 7.91 Hz, 2 H), 5.12−5.20 (m, 2 H), 2.32 (s, 3 H), 1.86−2.04 (m, 3 H), 1.72 (td, J = 8.76, 4.14 Hz, 1 H), 0.69−0.85 (m, 2 H), 0.44−0.60 (m, 2 H). [ES + MS] m/z = 475 (M + 1). HRMS calculated for $C_{21}H_{20}F_2N_6OS_2$, 475.118; found, 475.1181.

3-(2,6-Difluorobenzyl)-5-((5-(1-hydroxy-1-(4-methylthiazol-2-yl)ethyl)-1,3,4-thiadiazol-2-ylamino)methyl)oxazolidin-2-one (15). In a 50 mL round-bottomed flask, 3-(2,6-difluorobenzyl)-5-(isothiocyanatomethyl)oxazolidin-2-one (100 mg, 0.35 mmol) and 2-hydroxy-2-(4-methylthiazol-2-yl)propanehydrazide (70.8 mg, 0.35 mmol) were taken in DCM (8 mL) under nitrogen. The resulting clear solution was stirred for 50 min. After completion of the reaction, the volatiles were evaporated to dryness to get *N*-((3-(2,6-difluorobenzyl)-2-oxooxazolidin-5-yl)methyl)-2-(2-hydroxy-2-(4-methylthiazol-2-yl)propanoyl)hydrazinecarbothioamide (110 mg, 64.4%) as a solid. This solid was taken in concd H_2SO_4 (5 mL) and stirred at RT for 3 h. While stirring, the suspension turned to clear solution. LCMS showed the required mass after 25 min. Reaction was neutralized slowly with aqueous ammonia at 0 °C. The solution was diluted with water and extracted with DCM. The organic layer was separated and washed with water and brine solution. The organic layer was separated, dried over sodium sulfate, and concentrated. The crude compound was purified by reverse phase purification system to get product 3-(2,6-difluorobenzyl)-5-((5-(1-hydroxy-1-(4-methylthiazol-2-yl)ethyl)-1,3,4-thiadiazol-2-ylamino)methyl)oxazolidin-2-one (140 mg, 72.7%) as a solid. ^{1}H NMR (300 MHz, DMSO-d_6) δ ppm 7.94 (t, J = 5.75 Hz, 1 H), 7.35−7.51 (m, 1 H), 7.28 (s, 1 H), 7.21 (dd, J = 4.05, 1.04 Hz, 1 H), 7.11 (q, J = 8.29 Hz, 2 H), 4.67 (dd, J = 8.10, 5.65 Hz, 1 H), 4.42 (d, J = 7.72 Hz, 2 H), 3.42−3.57 (m, 3 H), 3.14−3.24 (m, 1 H), 2.31 (s, 3 H), 1.93 (s, 3 H). [ES + MS] m/z = 468 (M + 1). HRMS calculated for $C_{19}H_{19}F_2N_5O_3S_2$, 468.097; found, 468.0973.

1-(2,6-Difluorobenzyl)-*N*-(5-(1-hydroxy-1-(4-methylthiazol-2-yl)ethyl)-1,3,4-thiadiazol-2-yl)-1*H*-pyrazole-3-carboxamide (16). To 1-(2,6-difluorobenzyl)-1*H*-pyrazole-3-carbonyl isothiocyanate (100 mg, 0.36 mmol) and 2-hydroxy-2-(4-methylthiazol-2-yl)-propanehydrazide (72 mg, 0.36 mmol) was added DCM (5 mL) and then stirred for 30 min. The reaction mixture was concentrated under vacuum to get 1-(2,6-difluorobenzyl)-*N*-(2-(2-hydroxy-2-(4-methylthiazol-2-yl)propanoyl)hydrazinecarbonothioyl)-1*H*-pyrazole-3-carboxamide (170 mg, 99%) as a solid. [ES + MS] m/z = 481 (M + 1). In a 25 mL of RB flask, 1-(2,6-difluorobenzyl)-*N*-(2-(2-hydroxy-2-(4-methylthiazol-2-yl)propanoyl)hydrazinecarbonothioyl)-1*H*-pyrazole-3-carboxamide (310 mg, 0.65 mmol) was added followed by concd sulfuric acid (2 mL) and stirred for 30 min. The reaction mixture was neutralized carefully with aqueous ammonia solution at 0 °C. The reaction mixture was extracted with DCM, and the combined organic layer was washed with water and brine solution, dried over sodium sulfate, and concentrated. The crude was purified by column chromatography and then triturated with methanol:diethyl ether mixture to get 1-(2,6-difluorobenzyl)-*N*-(5-(1-hydroxy-1-(4-methylthiazol-2-yl)ethyl)-1,3,4-thiadiazol-2-yl)-1*H*-pyrazole-3-carboxamide (150 mg, 50.3%) as a solid. ^{1}H NMR (300 MHz, DMSO-d_6) δ ppm 7.98 (d, J = 2.3 Hz, 1H), 7.44−7.56 (m, 2H), 7.12−7.25 (m, 3H), 7.05 (d, J = 2.5 Hz, 1H), 5.51 (s, 2H), 2.30 (s, 3H), 2.02 (s, 3H). [ES + MS] m/z = 463 (M + 1). HRMS calculated for $C_{19}H_{16}F_2N_6O_2S_2$, 463.08169; found, 463.0803

■ ASSOCIATED CONTENT

Ⓢ Supporting Information

Details of the synthesis of all compounds, details of structure determination, and details of biological assays. This material is available free of charge via the Internet at http://pubs.acs.org.

Accession Codes

The atomic coordinates and structure factors for InhA in complex with **7** and **11** have been deposited in the Protein Data Bank (pdb accession codes 4bpq and 4bpr, respectively) along with structure factors and detailed experimental statistics.

■ AUTHOR INFORMATION

Corresponding Authors

*Phone: +91 080 23621212. Fax: +91 080 23621214. E-mail: pravin.shirude@astrazeneca.com.

*Phone: +44 1625 040376. E-mail: jon.read@astrazeneca.com.

Notes

The authors declare no competing financial interest.

■ ACKNOWLEDGMENTS

We thank the analytical support provided by S. Rudrapatna and analytical team. Our sincere thanks to the Microbiology, Target Biology, DMPK, and Safety team for technical support in various assays. We would like to thank our colleagues in the screening, protein supply, and characterization groups in Discovery Sciences, AstraZeneca. We also thank V. Balasubramanian, R. Tommasi, M. Perros, V. Hosagrahara, P. Iyer, and S. Narayanan for their constant inspiration, support, and encouragement.

■ ABBREVIATIONS USED

TB, tuberculosis; Mtb, *Mycobacterium tuberculosis*; ACPER, acyl carrier protein enoyl reductase; ACP, acyl carrier protein; INH, isoniazid; *inhA*, structural gene of acyl carrier protein enoyl reductase in *Mycobacterium tuberculosis*; InhA, *Mycobacterium tuberculosis* acyl carrier protein enoyl reductase; KatG, *Mycobacterium tuberculosis* catalase-peroxidase; NAD, nicotina-

mide adenine dinucleotide; NAD^+, oxidized nicotinamide adenine dinucleotide; NADH, reduced nicotinamide adenine dinucleotide; MIC, minimal inhibitory concentration; CYP, cytochrome P450; ITC, iso-thermal titration calorimetry; SPR, surface plasmon resonance; SAR, structure−activity relationships; DMPK, drug metabolism and pharmacokinetics; PPB, plasma protein binding; CL, clearance; LBF, liver blood flow; MMIC, mammalian cytotoxicity

REFERENCES

(1) *Global Tuberculosis Control: Surveillance, Planning, Financing*; World Health Organization: Geneva, Switzerland, 2011.

(2) Lu, H.; Tonge, P. J. Inhibitors of FabI, an Enzyme Drug Target in the Bacterial Fatty Acid Biosynthesis Pathway. *Acc. Chem. Res.* **2008**, *41*, 11−20.

(3) McDevitt, D.; Rosenberg, M. Exploiting genomics to discover new antibiotics. *Trends Microbiol.* **2001**, *9*, 611−617.

(4) Payne, D. J.; Warren, P. V.; Holmes, D. J.; Ji, Y.; Lonsdale, J. T. Bacterial fatty-acid biosynthesis: A genomics-driven target for antibacterial drug discovery. *Drug Discovery Today* **2001**, *6*, 537−544.

(5) Lamichhane, G. Novel targets in M. tuberculosis: search for new drugs. *Trends Mol. Med.* **2011**, *17*, 25−33.

(6) Rawat, R.; Whitty, A.; Tonge, P. J. The isoniazid-NAD adduct is a slow, tight-binding inhibitor of InhA, the *Mycobacterium tuberculosis* enoyl reductase: adduct affinity and drug resistance. *Proc. Natl. Acad. Sci. U. S. A.* **2003**, *100*, 13881−13886.

(7) Vilcheze, C.; Jacobs, W. R. The Mechanism of Isoniazid Killing: Clarity Through the Scope of Genetics. *Annu. Rev. Microbiol.* **2007**, *61*, 35−50.

(8) Banerjee, A.; Dubnau, E.; Quemard, A.; Balasubramanian, V.; Um, K. S.; Wilson, T.; Collins, D.; de Lisle, G.; Jacobs, W. R., Jr. *inhA*, a gene encoding a target for isoniazid and ethionamide in *Mycobacterium tuberculosis*. *Science* **1994**, *14*, 227−230.

(9) Davis, M. C.; Franzblau, S. G.; Martin, A. R. Syntheses and evaluation of benzodiazaborine compounds against *M. tuberculosis* $H_{37}R_v$ in vitro. *Bioorg. Med. Chem. Lett.* **1998**, *8*, 843−846.

(10) Lipinski, C. A.; Lombardo, F.; Dominy, B. W.; Feeney, P. J. Experimental and computational approaches to estimate solubility and permeability in drug discovery and development settings. *Adv. Drug Delivery Rev.* **2001**, *46*, 3−26.

(11) Hartkoorn, R. C.; Sala, C.; Neres, J.; Pojer, F.; Magnet, S.; Mukherjee, R.; Uplekar, S.; Boy-Röttger, S.; Altmann, K. H.; Cole, S. T. Towards a new tuberculosis drug: pyridomycin—nature's isoniazid. *EMBO Mol. Med.* **2012**, *4*, 1032−1042.

(12) Rafferty, J. B.; Simon, J. W.; Baldock, C.; Artymiuk, P. J.; Baker, P. J.; Stuitje, A. R.; Slabas, A. R.; Rice, D. W. Common themes in redox chemistry emerge from the X-ray structure of oilseed rape (*Brassica napus*) enoyl acyl carrier protein reductase. *Structure* **1995**, *3*, 927−938.

(13) Kuo, M. R.; Morbidoni, H. R.; Alland, D.; Sneddon, S. F.; Gourlie, B. B.; Staveski, M. M.; Leonard, M.; Gregory, J. S.; Janjigian, A. D.; Yee, C.; Musser, J. M.; Kreiswirth, B.; Iwamoto, H.; Perozzo, R.; Jacobs, W. R.; Sacchettini, J. C.; Fidock, D. A. Targeting tuberculosis and malaria through inhibition of enoyl reductase: compound activity and structural data. *J. Biol. Chem.* **2003**, *278*, 20851−20859.

(14) Pan, P.; Tonge, P. J. Targeting InhA, the FASII Enoyl-ACP Reductase: SAR Studies on Novel Inhibitor Scaffolds. *Curr. Top. Med. Chem.* **2012**, *12*, 672−693.

(15) Ballell Pages, L.; Castro Pichel, J.; Fernandez Menendez, R.; Fernandez Velando, E. P.; Gonzalez Del Valle, S.; Mendoza Losana, A.; Wolfendale, M. J. (Pyrazol-3-yl)-1,3,4-thiadiazole-2-amine and (Pyrazol-3-yl)-1,3,4-thiazole-2-amine Compounds. PCT publication No. WO 2010/118852 A1, 2010.

(16) Castro Pichel, J.; Fernandez Menendez, R.; Fernandez Velando, E. P.; Gonzalez Del Valle, S.; Mallo-Rubio, A. 3-Amino-Pyrazole Derivatives Useful Against Tuberculosis. PCT publication No. WO 2012/049161 A1, 2012.

(17) Ledź, P. S.; Śledź, P.; Lang, S.; Stubbs, C. J.; Abell, C. High-Throughput Interrogation of Ligand Binding Mode Using a Fluorescence-Based Assay. *Angew. Chem., Int. Ed.* **2012**, *51*, 7680−7683.

(18) Parikh, S. L.; Moynihan, D. P.; Xiao, G.; Tonge, P. J. Roles of Tyrosine 158 and Lysine 165 in the catalytic mechanism of InhA, the Enoyl-ACP Reductase from *Mycobacterium tuberculosis*. *Biochemistry* **1999**, *38*, 13623−13634.

(19) Vilchèze, C.; Weisbrod, T. R.; Chen, B.; Kremer, L.; Hazbón, M. H.; Wang, F.; Alland, D.; Sacchettini, J. C.; Jacobs, W. R., Jr. Altered $NADH/NAD^+$ ratio mediates coresistance to isoniazid and ethionamide in mycobacteria. *Antimicrob. Agents Chemother.* **2005**, *49*, 708−720.

(20) Luckner, S. R.; Liu, N.; Am Ende, C. W.; Tonge, P. J.; Kisker, C. A slow, tight binding inhibitor of InhA, the enoyl-acyl carrier protein reductase from *Mycobacterium tuberculosis*. *J. Biol. Chem.* **2010**, *285*, 14330−14337.

(21) Rozwarski, D. A.; Vilcheze, C.; Sugantino, M.; Bittman, R.; Sacchettini, J. C. Crystal structure of the *Mycobacterium tuberculosis* enoyl-ACP reductase, InhA, in complex with NAD+ and a C16 fatty acyl substrate. *J. Biol. Chem.* **1999**, *274*, 15582−15589.

(22) He, X.; Alian, A.; Stroud, R.; Ortiz de Montellano, P. R. Pyrrolidine Carboxamides as a Novel Class of Inhibitors of Enoyl Acyl Carrier Protein Reductase from *Mycobacterium tuberculosis*. *J. Med. Chem.* **2006**, *49*, 6308−6323.

(23) Sullivan, T. J.; Truglio, J. J.; Boyne, M. E.; Novichenok, P.; Zhang, X.; Stratton, C.; Li, H. J.; Kaur, T.; Amin, A.; Johnson, F.; Slayden, R. A.; Kisker, C.; Tonge, P. J. High Affinity InhA Inhibitors with Activity against Drug-Resistant Strains of *Mycobacterium tuberculosis*. *ACS Chem. Biol.* **2006**, *1*, 43−53.

(24) Chang, A.; Schiebel, J.; Yu, W.; Bommineni, G. R.; Pan, P.; Baxter, M. V.; Khanna, A.; Sotriffer, C. A.; Kisker, C.; Tonge, P. J. Rational Optimization of Drug-Target Residence Time: Insights from Inhibitor Binding to the *Staphylococcus aureus* FabI Enzyme-Product Complex. *Biochemistry* **2013**, *52*, 4217−4228.

(25) Dessen, A.; Quemard, A.; Blanchard, J. S.; Jacobs, W. R., Jr.; Sacchettini, J. C. Crystal structure and function of the isoniazid target of *Mycobacterium tuberculosis*. *Science* **1995**, *267*, 1638−1641.

(26) Schiebel, J.; Chang, A.; Lu, H.; Baxter, M. V.; Tonge, P. J.; Kisker, C. *Staphylococcus aureus* FabI: Inhibition, Substrate Recognition and Potential Implications for In Vivo Essentiality. *Structure* **2012**, *9*, 802−813.